Separation Science and Technology
Publication details, including instructions for authors and subscription information:
http://www.informaworld.com/smpp/title~content=t713708471

MAGNETIC FIELD ORIENTATION AND SPATIAL EFFECTS ON THE RETENTION OF PARAMAGNETIC NANOPARTICLES WITH MAGNETITE

Armin D. Ebner[a]; Harry J. Ploehn[a]; James A. Ritter[a]
[a] Department of Chemical Engineering, Swearingen Engineering Center, University of South Carolina, Columbia, SC, U.S.A.

Online publication date: 12 February 2002

To cite this Article Ebner, Armin D. , Ploehn, Harry J. and Ritter, James A.(2002) 'MAGNETIC FIELD ORIENTATION AND SPATIAL EFFECTS ON THE RETENTION OF PARAMAGNETIC NANOPARTICLES WITH MAGNETITE', Separation Science and Technology, 37: 16, 3727 — 3753
To link to this Article: DOI: 10.1081/SS-120014823
URL: http://dx.doi.org/10.1081/SS-120014823

MARCEL DEKKER, INC. • 270 MADISON AVENUE • NEW YORK, NY 10016

SEPARATION SCIENCE AND TECHNOLOGY
Vol. 37, No. 16, pp. 3727–3753, 2002

MAGNETIC FIELD ORIENTATION AND SPATIAL EFFECTS ON THE RETENTION OF PARAMAGNETIC NANOPARTICLES WITH MAGNETITE

Armin D. Ebner, Harry J. Ploehn, and James A. Ritter*

Department of Chemical Engineering, Swearingen Engineering Center, University of South Carolina, Columbia, SC 29208

ABSTRACT

The magnetic force exerted on a paramagnetic nanoparticle by a 3-D array of magnetite particles was investigated to extend previous work that only involved one magnetite particle. The separation between the magnetite particles in the array, the orientation of the magnetic field, and the distance between the nanoparticle and the surface of the magnetite array were studied. At magnetite particle separations of less than two magnetite diameters, a reduction in the net force on the nanoparticle compared to that associated with a single magnetite particle was realized due to the overlapping behavior of the magnetic fields of the magnetite array. The net force was still strong to overcome thermal (Brownian) motion and attract and retain the nanoparticle.

*Corresponding author. Fax: (803) 777-8265; E-mail: ritter@engr.sc.edu

DOI: 10.1081/SS-120014823 0149-6395 (Print); 1520-5754 (Online)

MARCEL DEKKER, INC. • 270 MADISON AVENUE • NEW YORK, NY 10016

The magnetite array also gives rise to retention zones at any orientation of the magnetite field; this was not true of a single magnetite particle, which exhibited repulsive zones depending on the orientation of the field. When the separation between the magnetite particles was greater than two magnetite diameters, the effect of the array was lost and the nanoparticle interacted essentially with only one of the magnetite particles. The close proximity of the magnetite particles and the associated smoothing effect translated into long-range interactions that leveled off with distance between the nanoparticle and the array. Although too weak to retain the nanoparticle, they were suspected to be strong enough to retain much larger particles approaching the size of the array. These effects could be explained only by the fact that when the magnetite particles were closer to each other they started behaving as a single large particle. Overall, these results suggest that both nanoparticles and particles of the size the array can be attracted to and retained by a magnetic matrix comprising clusters of small and similarly sized magnetite particles.

Key Words: Magnetic forces; Colloidal forces; High gradient magnetic separation; Magnetite; Particles

INTRODUCTION

In recent years, researchers[1–4] have been exploring the use of magnetite as an alternative magnetically energizable high gradient magnetic separation (HGMS) element for the removal of particles. Due to its relatively large saturation magnetization and much smaller size than stainless steel wool, magnetite can be an effective magnetic element for the removal of even smaller paramagnetic particles. Moreover, magnetite is well known for its metal ion adsorptive properties, which also allows it to remove metals present in an ionic state that are not necessarily magnetic. The first experimental attempt to use magnetite in this fashion was presented in the work of Kochen and Navratil,[1] who utilized magnetic polyamine epichlorohydrin (MPE) resin beads coated with magnetite within a 0.3 T HGMS packed bed. With the MPE resin, a magnetic field of 0.3 T, and under very alkaline conditions (pH 12), they were able to effectively remove several times more colloidal plutonium and americium than with the more traditional stainless steel wool matrix. Shortly

thereafter, Ebner et al.[2–4] explored the feasibility and limitations of the HGMS process like that described by Kochen and Navratil.[1]

Ebner et al.[2–4] theoretically compared the magnetic force with Brownian and other naturally occurring forces (i.e., van der Waals and electrostatic) between a paramagnetic particle and magnetite under the influence of an external magnetic field and convective forces and qualitatively explained the experimental results obtained by Kochen and Navratil.[1] They also concluded that the removal of paramagnetic particles is perfectly feasible down to a radius of approximately 40 nm, as long as special precautions are taken, in terms of the electrolyte concentration, to overcome the strongly repulsive electrostatic force. In all these situations, however, the study was restricted to the limiting case of a paramagnetic nanoparticle and a single magnetite particle. Although insightful in showing the relative role of the forces involved when using magnetite in this type of separation process, studying interactions between only two particles raises an important question about the "smoothing" of the magnetic field gradient around a magnetite particle when it is surrounded by other neighboring magnetite particles of similar size.

Therefore, the objective here is to elucidate the effect of the magnetic force on a single paramagnetic nanoparticle by a 3-D array of 500 identically sized magnetite particles. Three relevant variables that affect the net force on the paramagnetic particle are investigated. These are the distance between the magnetite particles, the orientation of the magnetic field with respect to the interface of the magnetite particle array, and the vertical distance between the paramagnetic nanoparticle and the magnetite array. The net magnetic force is calculated and compared only to the force associated with random Brownian (thermal) motion to determine under what conditions magnetic attraction (i.e., retention) or repulsion of the paramagnetic nanoparticle occurs.

MODEL DEVELOPMENT

Figure 1a shows the array of equally sized magnetite particles consisting of $10 \times 10 \times 5$ magnetite units of radius r_m and a paramagnetic nanoparticle of radius r_p placed at any distance above the top layer of the magnetite particle array. The distances between all the magnetite particles in the array are identical and the magnetite particles are subjected to a magnetic field H_a that is inclined at an angle α with respect to the y-axis and lying parallel to the z–y plane. Figure 1b shows an augmented view of the region in the x–y plane within which the interactions between the array of magnetite spheres and the nanoparticle are calculated. The defined region in the x–y plane consists of a square of area $2r_m(1 + s) \times 2r_m(1 + s)$ bounded by the centers of the four innermost magnetite particles of the top layer, where the parameter s is the ratio between the surface-to-surface distance between the magnetite particles and their diameter.

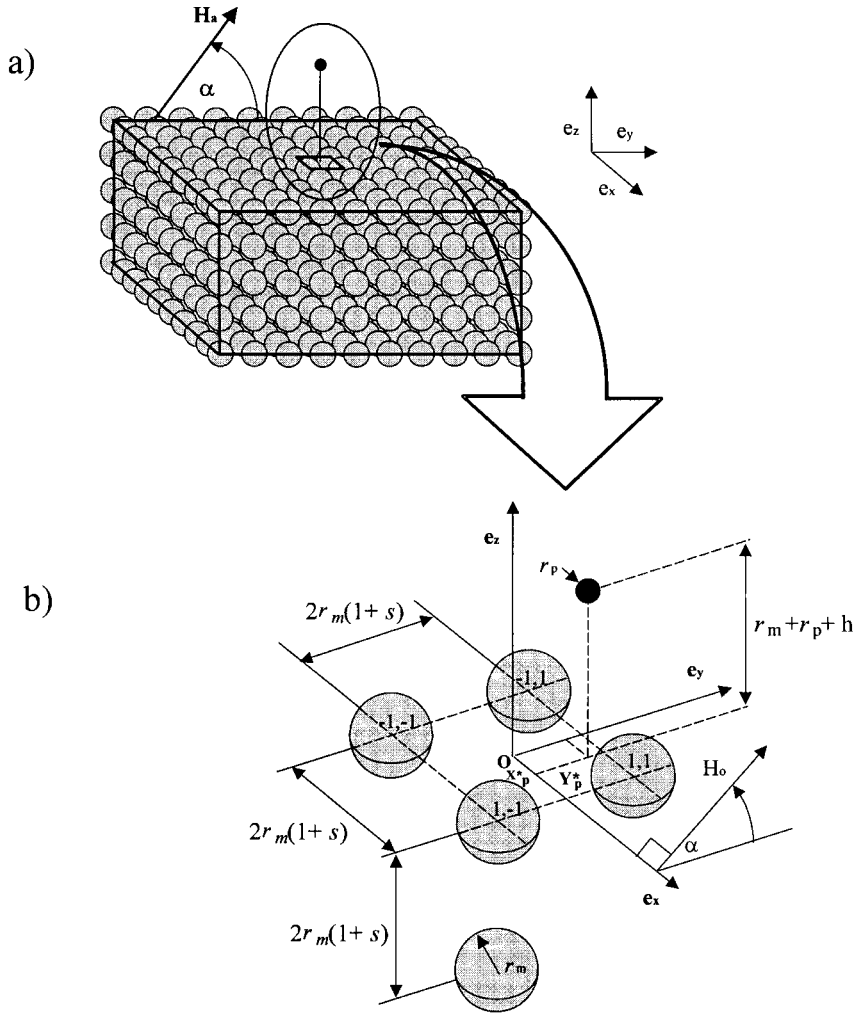

Figure 1. Schematic of (a) the 3-D array containing $10 \times 10 \times 5$ magnetite particles and a paramagnetic nanoparticle, and (b) close-up of the central rectangular region in the $x-y$ plane at the surface of the array where the magnetic interactions are calculated.

The nanoparticle is placed at a distance $r_m + r_p + h$, where h represents the surface-to-surface distance from the nanoparticle to the plane that is tangent to the top layer of the magnetite particles in the array and parallel to the $x-y$ plane. With the origin being defined at the center of the square, the Z_p^* coordinate of

the nanoparticle is given by

$$Z_{\mathrm{p}}^{*} = r_{\mathrm{m}} + r_{\mathrm{p}} + h \tag{1a}$$

with the X_{p}^{*} and Y_{p}^{*} coordinates restricted to the following limits

$$-r_{\mathrm{m}}(1+s) \le X_{\mathrm{p}}^{*} \le r_{\mathrm{m}}(1+s) \tag{1b}$$

$$-r_{\mathrm{m}}(1+s) \le Y_{\mathrm{p}}^{*} \le r_{\mathrm{m}}(1+s) \tag{1c}$$

For a magnetite particle i in the array, the coordinates are defined as

$$X_{\mathrm{m},i}^{*} = (-9 + 2(k_i - 1)) \times r_{\mathrm{m}}(1+s) \quad k_i = 1, 2 \ldots, 10 \tag{2a}$$

$$Y_{\mathrm{m},i}^{*} = (-9 + 2(l_i - 1)) \times r_{\mathrm{m}}(1+s) \quad l_i = 1, 2 \ldots, 10 \tag{2b}$$

$$Z_{\mathrm{m},i}^{*} = (-2(m_i - 1)) \times r_{\mathrm{m}}(1+s) \quad m_i = 1, 2 \ldots, 5 \tag{2c}$$

The net force on a single nanoparticle due to a 3-D array of magnetite particles is derived from the application of the superposition property of magnetic fields.[5–8] The expressions for the components of the magnetic force on a nanoparticle by a single magnetite particle are given by the well-known formula in spherical coordinates:[2]

$$F_{\mathrm{m},r} = -V_{\mathrm{p}}\mu_0(\chi_{\mathrm{p}} - \chi_{\mathrm{m}})\left(\frac{r_{\mathrm{m}}^3 M_{\mathrm{s}}}{r^4}\right) \times \left[2\left(H_{\mathrm{a}} + \frac{2r_{\mathrm{m}}^3}{3r^3}M_{\mathrm{s}}\right)\cos^2\theta + \left(-H_{\mathrm{a}} + \frac{r_{\mathrm{m}}^3}{3r^3}M_{\mathrm{s}}\right)\sin^2\theta\right] \tag{3a}$$

$$F_{\mathrm{m},\theta} = V_{\mathrm{p}}\mu_0(\chi_{\mathrm{p}} - \chi_{\mathrm{m}}) \times \frac{\cos\theta\sin\theta}{r}\left[-\left(H_{\mathrm{a}} + \frac{2r_{\mathrm{m}}^3}{3r^3}M_{\mathrm{s}}\right)^2 + \left(-H_{\mathrm{a}} + \frac{r_{\mathrm{m}}^3}{3r^3}M_{\mathrm{s}}\right)^2\right] \tag{3b}$$

where θ is the angle formed by the line containing the center of the magnetite particle and parallel to the applied field H_{a}, and the lines of centers of the nanoparticle and the magnetite particle, r is the center to center separation between these two particles, M_{s} is the saturation magnetization of the magnetite particle, V_{p} is the volume of the nanoparticle, and χ_{p} and χ_{m} are the volumetric susceptibilities of the magnetic particle and the medium, respectively. However, because the expressions given in Eqs. (3a) and (3b) are in spherical coordinates, they are origin dependent and thus they cannot be used directly to calculate the net

force of the array on the nanoparticle. This problem is resolved if each of the magnetite–paramagnetic particle interactions defined according to the spherical coordinate system of Eqs. (3a) and (3b) are transformed into the common Cartesian coordinate system presented in Fig. 1. In this way, the superposition principle can be used to sum directly the components of all the individual pair interactions. After this transformation, the net magnetic force is given simply by

$$F_{\mathrm{m},j} = \sum_{i=1}^{N} F_{\mathrm{m},i,j}, \quad j = x, y, \text{ or } z \tag{4}$$

where $F_{\mathrm{m},i,j}$ represents the component of the magnetic force due to magnetite particle i interacting with the nanoparticle along direction j (i.e., $j = x, y,$ or z) with N being the total number of magnetite particles in the system. To carry out the transformation from the spherical to the Cartesian coordinate system several steps are needed.

First, for each interaction between the nanoparticle and magnetite particle i in the array, the origin of the Cartesian coordinates that define the position of the nanoparticle (i.e., X_{p}^*, Y_{p}^*, and Z_{p}^* in Fig. 2a) is relocated to the center of magnetite particle i. Hence, for each individual case, the new coordinates of the nanoparticle, X_i^*, Y_i^*, and Z_i^* with respect to magnetite particle i are given by

$$X_i^* = X_{\mathrm{p}}^* - X_{\mathrm{m},i}^* \tag{5a}$$

$$Y_i^* = Y_{\mathrm{p}}^* - Y_{\mathrm{m},i}^* \tag{5b}$$

$$Z_i^* = Z_{\mathrm{p}}^* - Z_{\mathrm{m},i}^* \tag{5c}$$

and shown in Fig. 2b. Now, as stated earlier, the field, H_{a}, lies in the y–z plane and is inclined with an angle α with respect to the y-axis (i.e., angle $1 - \alpha$ with respect to the z-axis). Under these circumstances, the field is not aligned with the z-axis so that well-known formulas to convert between the spherical coordinate system mentioned above and that represented by Eqs. (5a)–(5c) cannot be used directly. To cope with this problem, an auxiliary system of Cartesian coordinates is defined such that its new z'-axis is set parallel to the applied field while keeping its x'-axis coincident to that of the Cartesian coordinate system in Fig. 2b (see Fig. 3). In other words, the new Cartesian coordinate system is rotated clockwise, $1 - \alpha$, around the x-axis of the old Cartesian system shown in Fig. 2b, i.e., the components of the magnetic force of the old Cartesian coordinate system (i.e., $F_{\mathrm{m},i,x}$, $F_{\mathrm{m},i,y}$, $F_{\mathrm{m},i,z}$) are now related to those of the new auxiliary coordinate

MARCEL DEKKER, INC. • 270 MADISON AVENUE • NEW YORK, NY 10016

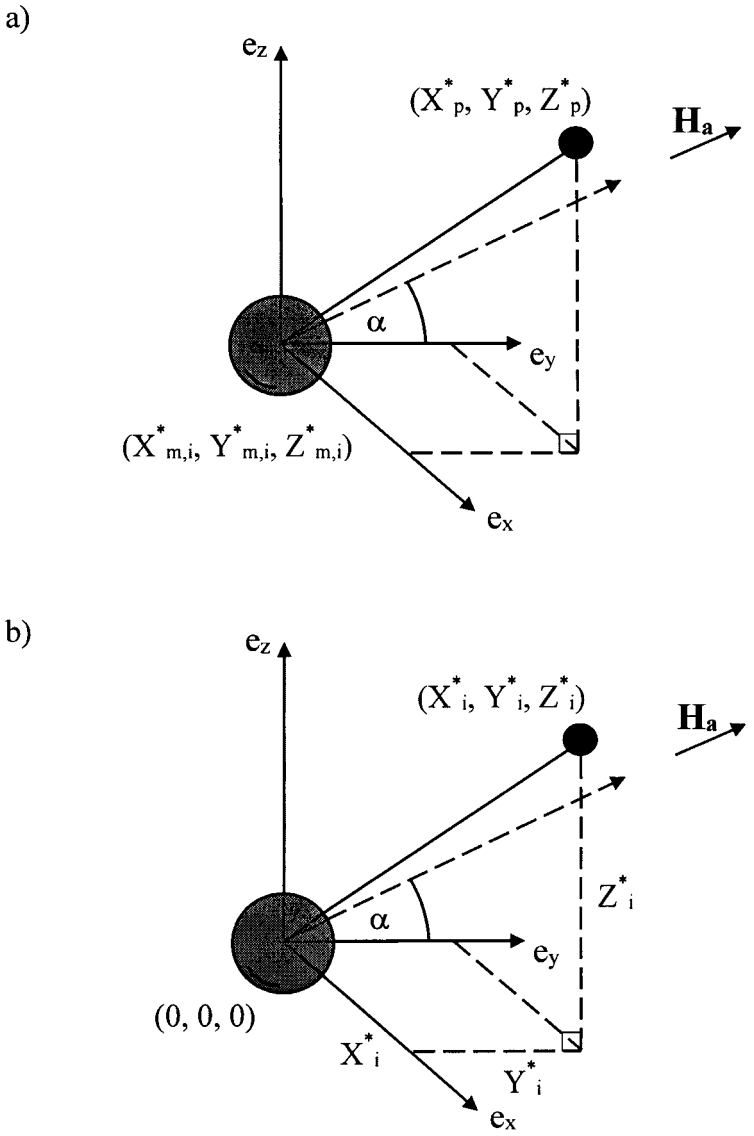

Figure 2. Representations of the paramagnetic nanoparticle and magnetite particle *i* in a Cartesian coordinate system with the origin located at (a) the center of the square defined in Fig. 1b, and (b) the center of magnetite particle *i* where $\mathbf{H}_a$ is parallel to the $y-z$ plane and inclined at an angle α with respect to the y-axis.

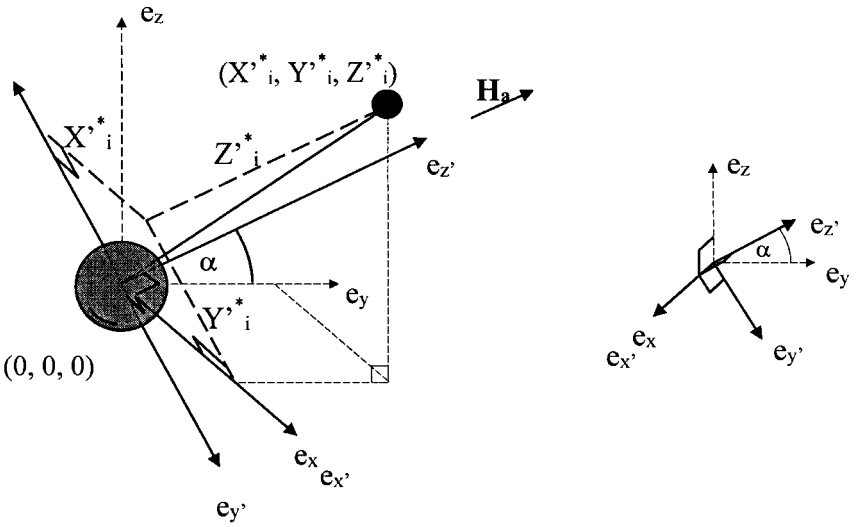

Figure 3. Representation of the paramagnetic nanoparticle and magnetite particle i in an auxiliary Cartesian coordinate system that is rotated clockwise $1 - \alpha$ around the x-axis so that the new z'-axis is parallel to the magnetic field $\mathbf{H}_a$.

system (i.e., $F_{\mathrm{m},i,x'}, F_{\mathrm{m},i,y'}, F_{\mathrm{m},i,z'}$) through the application of the rotation matrix:

$$\begin{bmatrix} F_{\mathrm{m},i,x} \\ F_{\mathrm{m},i,y} \\ F_{\mathrm{m},i,z} \end{bmatrix}^{\mathrm{T}} = \begin{bmatrix} F_{\mathrm{m},i,x'} \\ F_{\mathrm{m},i,y'} \\ F_{\mathrm{m},i,z'} \end{bmatrix}^{\mathrm{T}} \begin{bmatrix} 1 & 0 & 0 \\ 0 & \sin\alpha & -\cos\alpha \\ 0 & \cos\alpha & \sin\alpha \end{bmatrix} \tag{6}$$

Once this new Cartesian system is defined, adequate assignments for θ_i, ϕ_i, and r_i can be easily done, as shown in Fig. 4; and the components of the force in Eqs. (3a) and (3b) (i.e., $F_{\mathrm{m},i,r}$, $F_{\mathrm{m},i,\theta}$) can be used to obtain those of the auxiliary coordinate system according to the familiar transformation:

$$\begin{bmatrix} F_{\mathrm{m},i,x'} \\ F_{\mathrm{m},i,y'} \\ F_{\mathrm{m},i,z'} \end{bmatrix}^{\mathrm{T}} = \begin{bmatrix} F_{\mathrm{m},i,r} \\ F_{\mathrm{m},i,\theta} \\ 0 \end{bmatrix}^{\mathrm{T}} \begin{bmatrix} \sin\theta_i\cos\phi_i & \sin\theta_i\sin\phi_i & \cos\theta_i \\ \cos\theta_i\cos\phi_i & \cos\theta_i\sin\phi_i & -\sin\theta_i \\ -\sin\phi_i & \cos\phi_i & 0 \end{bmatrix} \tag{7}$$

Equations (6) and (7) now provide the necessary relationships that transform the components of the magnetic force in Eqs. (3a) and (3b) into the Cartesian coordinate system shown in Fig. 1. However, the angles θ and ϕ, as well as the distance between the centers r, are still not known a priori and must be

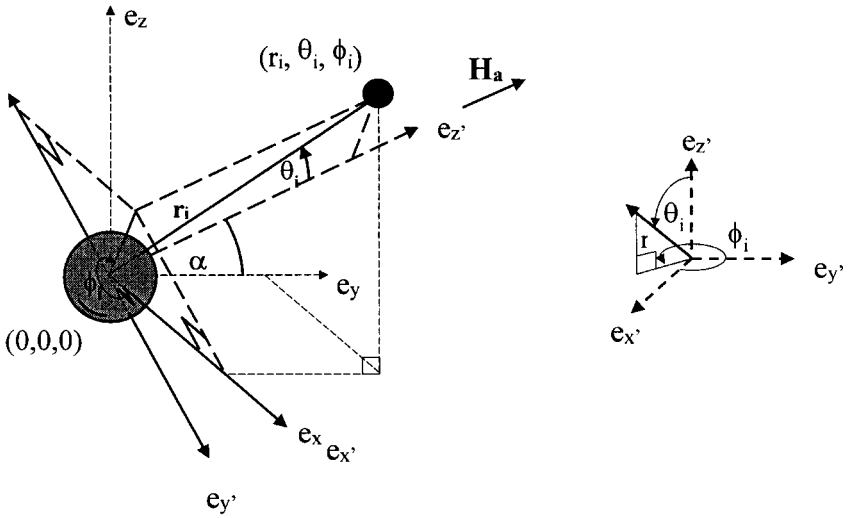

Figure 4. Representation of the paramagnetic nanoparticle and magnetite particle *i* in a spherical coordinate system defined relative to the auxiliary Cartesian coordinate system.

expressed in terms of known variables (i.e., X_i^*, Y_i^*, Z_i^*, and α). Figure 5 depicts a planar polygon conformed by corners A, B, C, and D that is contained in a plane that is parallel to the y–z plane. The points E and F, inside AB and BC, respectively, are inserted so that the straight lines EC and FD are, respectively, parallel to sides DA and AB. With this arrangement, it is easy to show that the angles ECB and FDC are identical to α and that the following trigonometric relationships for θ_i and ϕ_i naturally follow:

$$\cos\theta_i = \frac{\overline{\mathrm{AB}}}{r_i} = \frac{Z_i^* \sin\alpha + Y_i^* \cos\alpha}{r_i} \tag{8}$$

$$\sin\theta_i = \sqrt{1 - \cos^2\theta_i} \tag{9}$$

$$\cos\phi_i = \frac{\overline{\mathrm{OD}}}{\overline{\mathrm{AO}}} = \frac{X_i^*}{r_i \sin\theta_i} \tag{10}$$

$$\sin\phi_i = \frac{\overline{\mathrm{AD}}}{\overline{\mathrm{AO}}} = -\frac{Z_i^* \cos\alpha - Y_i^* \sin\alpha}{r_i \sin\theta_i} \tag{11}$$

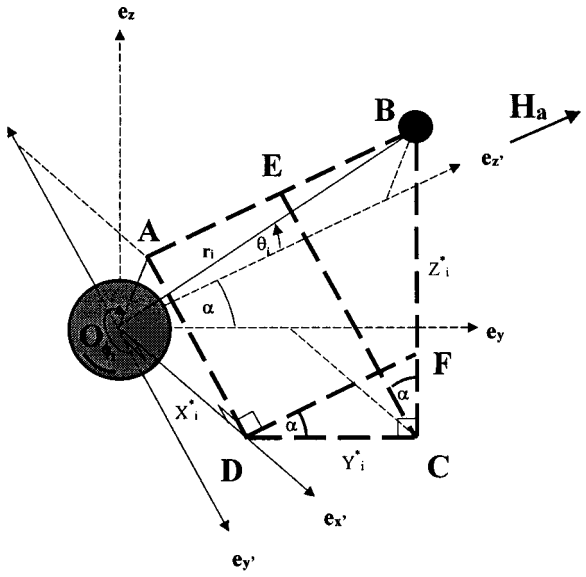

Figure 5. Representation of the paramagnetic nanoparticle and magnetite particle i highlighting polygon ABCD, which is parallel to the y–z plane and used for determining Eqs. (8)–(11).

where

$$r_i = (X_i^{*2} + Y_i^{*2} + Z_i^{*2})^{0.5} \tag{12}$$

Note that the expression presented in Eq. (11) is preferred for evaluating $\sin\phi_i$ over the traditional trigonometric identity $\sin\phi_i = \sqrt{1 - \cos^2\phi_i}$ to cope with the sign problems that arise from the symmetry of the above vectorial transformations.

In summary, the components of the net force on the nanoparticle (i.e., $F_{\mathrm{m},x}$, $F_{\mathrm{m},y}$, $F_{\mathrm{m},z}$) created by the magnetite particle array are calculated from the sum of the corresponding components of the individual magnetite particle and nanoparticle pair interactions (i.e., $F_{\mathrm{m},i,x}$, $F_{\mathrm{m},i,y}$, $F_{\mathrm{m},i,z}$), which are obtained as follows. First, with s, h, r_{m}, and r_{p} specified and based on the Cartesian coordinate system of Fig. 1b, all the coordinates of the magnetite particles (i.e., $X^*_{\mathrm{m},i}$, $Y^*_{\mathrm{m},i}$, and $Z^*_{\mathrm{m},i}$) and the nanoparticle (i.e., X^*_{p}, Y^*_{p}, and Z^*_{p}) are determined from Eqs. (1a)–(1c), (2a)–(2c). Then, for every nanoparticle and magnetite particle i pair, the origin is relocated at the coordinates of the magnetite particle (i.e., at $X^*_{\mathrm{m},i}$, $Y^*_{\mathrm{m},i}$, and $Z^*_{\mathrm{m},i}$), which defines new coordinates for the nanoparticle

(i.e., X_i^*, Y_i^*, and Z_i^*) according to Eqs. (5a)–(5c). With $X_{\mathrm{m},i}^*$, $Y_{\mathrm{m},i}^*$, and $Z_{\mathrm{m},i}^*$ determined, and based on the spherical coordinate system depicted in Fig. 4, the trigonometric functions of θ_i and ϕ_i, and r_i are evaluated from Eqs. (8)–(12). Finally, the desired components $F_{\mathrm{m},i,x}$, $F_{\mathrm{m},i,y}$, and $F_{\mathrm{m},i,z}$ are obtained from the formulas given for $F_{\mathrm{m},i,\theta}$ and $F_{\mathrm{m},i,\phi}$ in Eqs. (3a) and (3b), after carrying out the linear transformation of Eq. (7) (which evaluates $F_{\mathrm{m},i,x'}$, $F_{\mathrm{m},i,y'}$, and $F_{\mathrm{m},i,z'}$) followed by the linear transformation of Eq. (6).

RESULTS AND DISCUSSION

As done in previous studies,[2–4] the forces here are evaluated in dimensionless form relative to the Brownian force by dividing their magnitude by $|k_{\mathrm{b}}T/a_{\mathrm{p}}|$, i.e.,

$$F_{\mathrm{m},j}^* = \left|\frac{a_{\mathrm{p}}}{kT}\right| F_{\mathrm{m},j} \tag{13}$$

When the magnitude of this dimensionless expression is $\gg 1$, the force on the nanoparticle is strong enough to overcome any thermal motion, and absolute value > 10 is considered strong enough to dominate the randomizing effect of the Brownian motion. Table 1 lists the values and ranges of the parameters utilized in this model. Four main variables are considered: the angle α, the distance h between the nanoparticle and the array, the distance between the magnetite particles s, and the variables x and y, which represent the x and y-coordinates of the nanoparticle in dimensionless terms, i.e.,

$$x = \frac{X_{\mathrm{p}}^*}{r_{\mathrm{m}}(1+s)} \tag{14a}$$

Table 1. Model Parameters and Ranges

Parameters	
α	0–90°
s	0.0–1.0
h (nm)	20–1,000
H_{a} (A m^{-1})	2,387,319
M_{s} (A m^{-1})	480,000
a_{p} (nm)	160
r_{m} (nm)	400
χ_{p}	250×10^{-6}
χ_{m}	13×10^{-6}

$$y = \frac{Y_p^*}{r_m(1+s)} \tag{14b}$$

All other parameters are kept constant. For simplicity, the four magnetite particles closest to the nanoparticle are referred to the location of their centers, according to these dimensionless x, y-coordinates, as shown in Fig. 1b. In addition, it is noteworthy that the magnetic susceptibility of the nanoparticle corresponds to a weak paramagnetic species like CuO or PuO_2.

Figures 6–8 show the variations of the components of the total magnetic force (i.e., dimensionless forms of $F_{m,x}$, $F_{m,y}$, and $F_{m,z}$, respectively) that is exerted on the nanoparticle as depicted in Fig. 1b and for different angles α of the field. The four corners of the x–y plane of the figures [i.e., coordinate points $(-1,-1)$, $(1,-1)$, $(1,1)$, and $(-1,1)$] represent the x–y dimensionless coordinates of the centers of each of the magnetite particles of Fig. 1b. These results correspond to $h = 20$ nm and $s = 0$, with all other parameters fixed at the values given in Table 1. The legend in each figure indicates the correspondence between the sign of the particular component being analyzed and its actual direction relative to the axis in the figure. The bold line on the surface of each 3-D plot represents the location of unstable equilibrium in the x–y plane. This is where the component of the total force on the nanoparticle is zero, but where the potential energy of the interaction is maximum, forcing the nanoparticle to move away from these positions in the direction of the components in question. In the particular case of the z-component (i.e., Fig. 8), the bold line represents the boundary between the repulsive (i.e., positive $F_{m,z}$) and attractive (i.e., negative $F_{m,z}$) regions for the nanoparticle.

As the direction of the applied field H_a changes from a parallel orientation to the y-axis (i.e., $\alpha = 0°$) to a parallel orientation to the z-axis (i.e., $\alpha = 90°$), the shape of the surface representing the z-component of the total force in Fig. 8 changes from a saddle-like shape (Fig. 8a) to a table-like shape (Fig. 8g). Each situation is characterized by a large zone in the x–y plane where attraction of the nanoparticle takes place. For the conditions investigated here, the attractive magnetic force in this zone is strong enough to overcome Brownian disruption (i.e., $F_{m,z}r_p/k_bT < -10$). These attractive zones persist irrespective of the angle of the applied field, especially along the lines connecting the magnetite particles placed at (x,y) coordinates $(1,-1)$ and $(-1,-1)$ with those placed at $(1,1)$ and $(-1,1)$, respectively. As α changes from 0 to 90°, these attractive zones move along these connecting lines from the mid point (i.e., at $y = 0$) towards the centers of the particles (i.e., at $y = -1$), which is where the attractive force reaches a maximum. The region surrounding the saddle point at (0,0) in Fig. 8a is also attractive for the nanoparticle and remains so while moving toward the $(0,-1)$ coordinate at inclination angles of the magnetic field as large as 60°

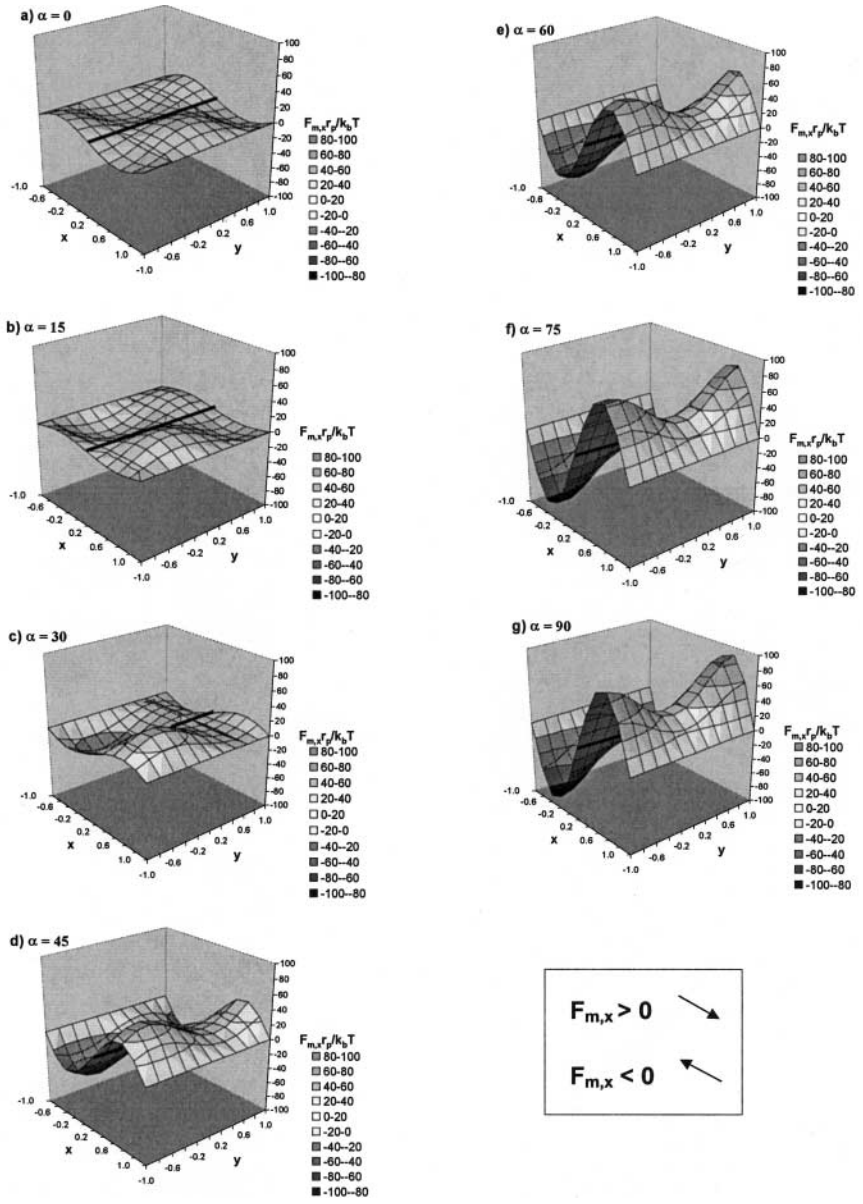

Figure 6. *x*-Component of the total magnetic force on the paramagnetic nanoparticle that is exerted by the array of magnetite particles within the square defined in Fig. 1b for different orientations of the magnetic field (i.e., α), and for $h = 20\,\text{nm}$ and $s = 0.0$. All other parameters are fixed and given in Table 1.

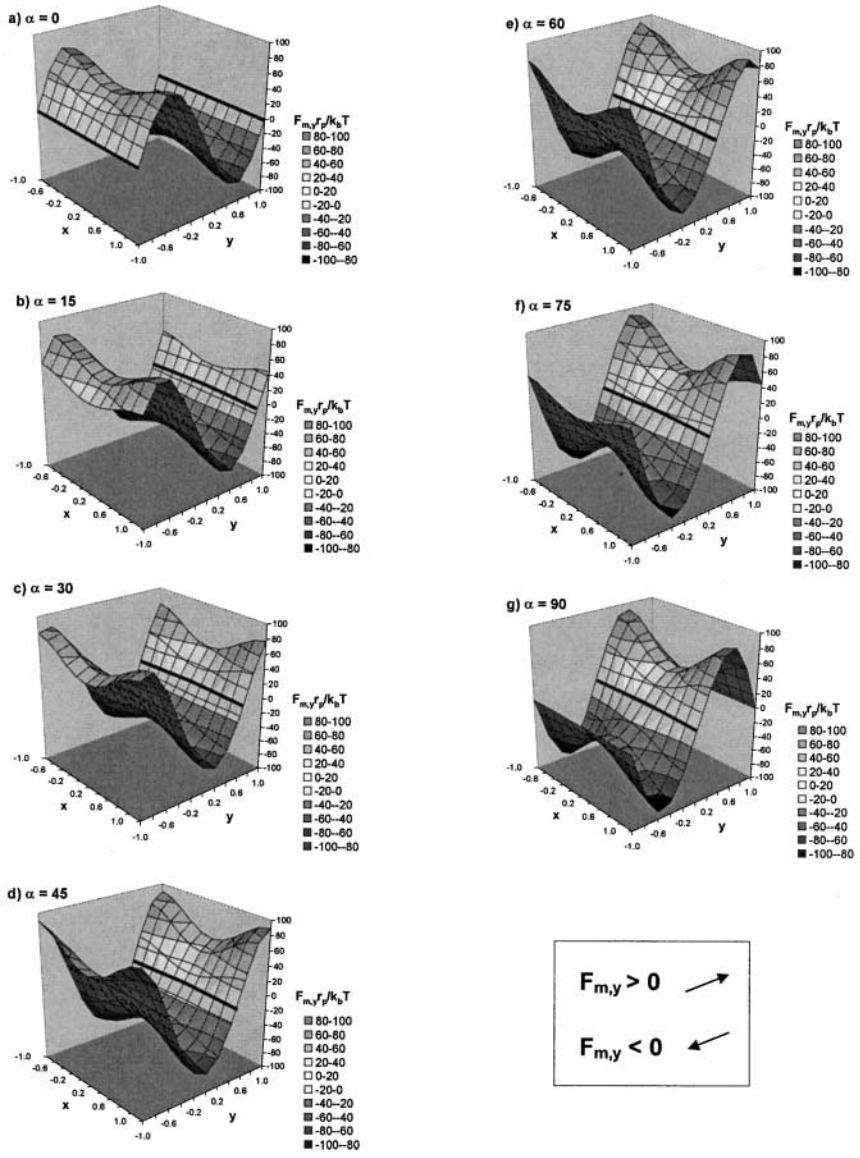

Figure 7. *y*-Component of the total magnetic force on the paramagnetic nanoparticle that is exerted by the array of magnetite particles within the square defined in Fig. 1b for different orientations of the magnetic field (i.e., α), and for $h = 20\,\text{nm}$ and $s = 0.0$. All other parameters are fixed and given in Table 1.

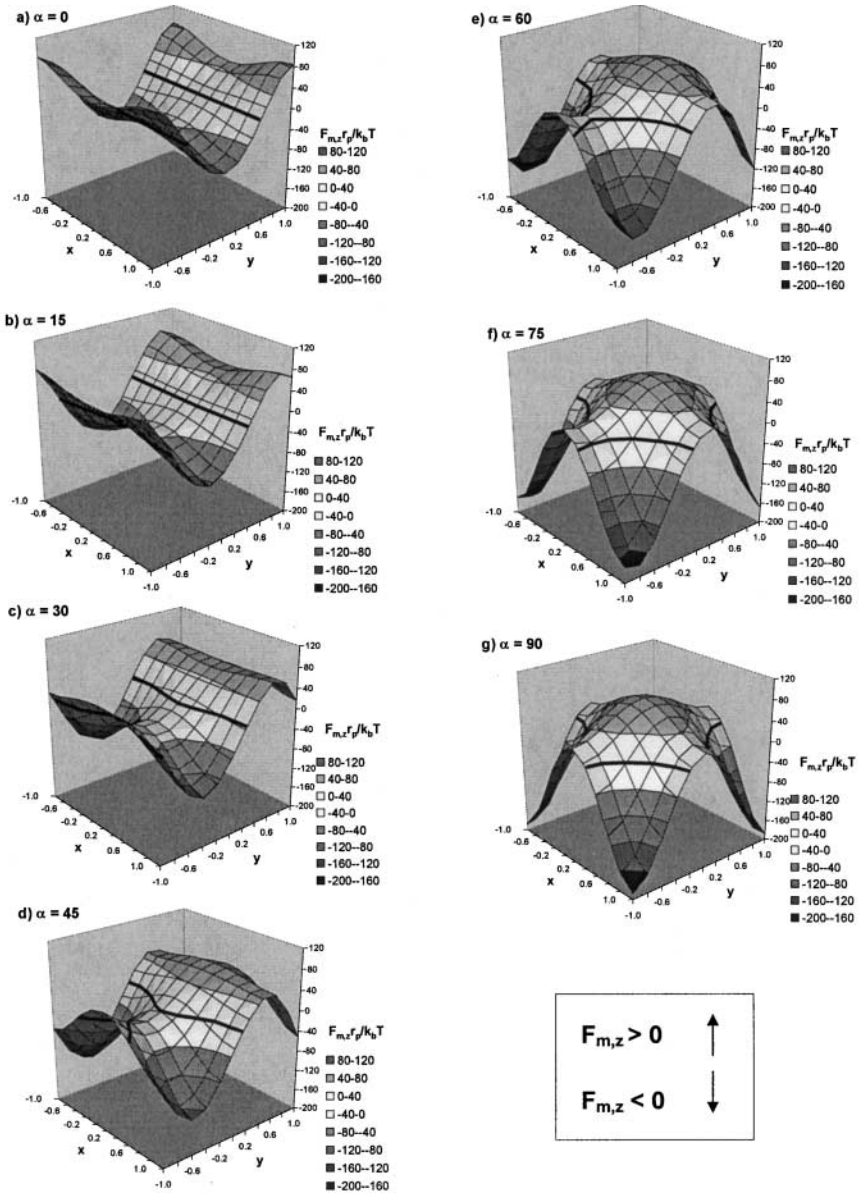

Figure 8. z-Component of the total magnetic force on the paramagnetic nanoparticle that is exerted by the array of magnetite particles within the square defined in Fig. 1b for different orientations of the magnetic field (i.e., α), and for $h = 20$ nm and $s = 0$. All other parameters are fixed and given in Table 1.

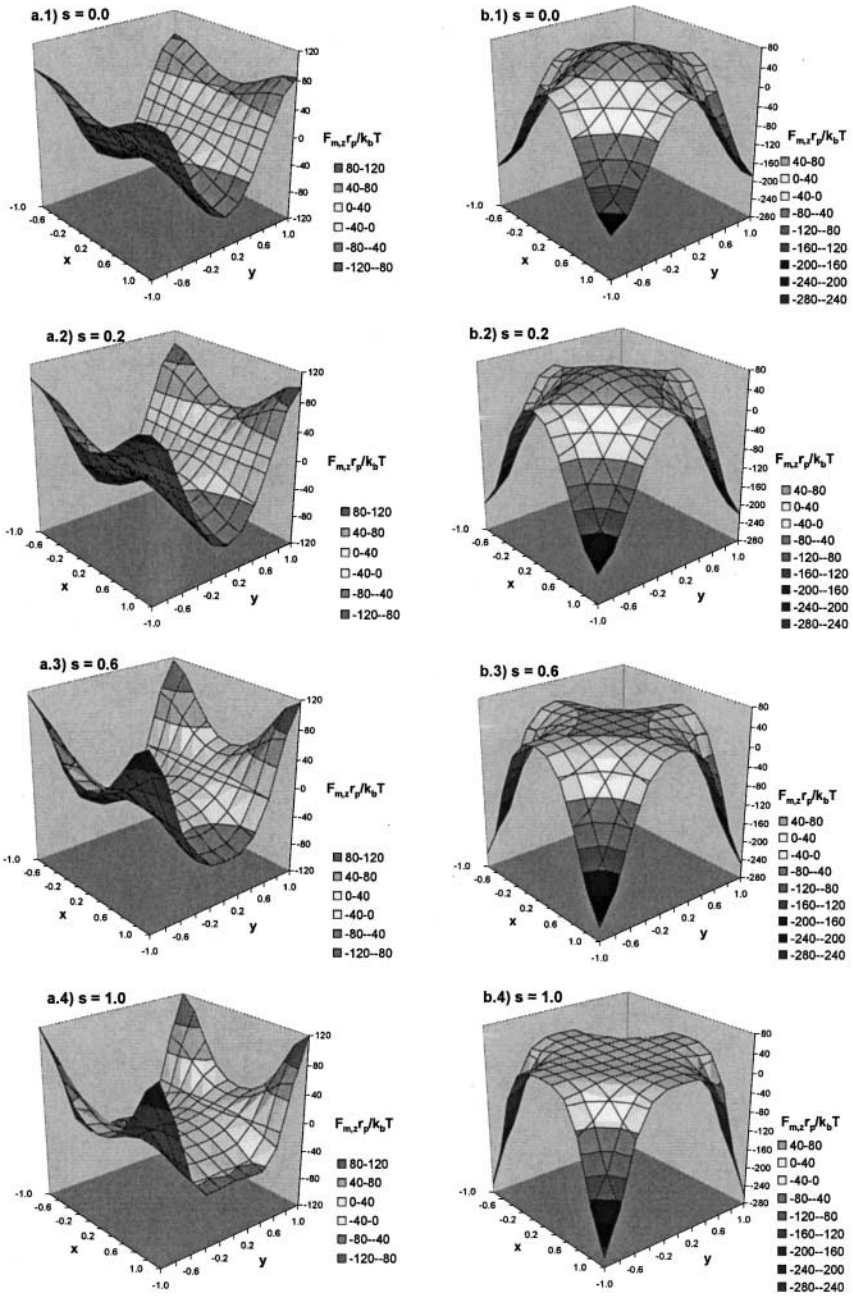

(see Fig. 8e). Figure 7 shows that the y-component of the magnetic force on the nanoparticle is stable for all the attractive regions described above, whereas the thick lines at $x = 0$ in Fig. 6 (x-component) indicate that at the regions around the saddle points of the z-component in Fig. 8, the nanoparticle experiences unstable equilibrium and tries to move away from them in the x-direction.

Figure 9 shows the variation of the z-component of the total force at different distances between the magnetite particles (i.e., $s = 0$, 0.2, 0.6, and 1.0), and for two different orientations of the applied field ($\alpha = 0$ and 90°). As the magnetite particles become farther apart, increasingly stronger repulsive (i.e., Fig. 9a) or attractive (i.e., Fig. 9b) forces are exerted on the nanoparticle when placed at the centers of the magnetite particles (i.e., at (1,1), (1, − 1), (− 1,1), and (− 1, − 1)). However, the opposite trend is observed when the nanoparticle is placed in the middle regions between the magnetite particles (i.e., at (0,1), (0, − 1), (1,0), (− 1,0), and (0,0)), where the force on the nanoparticle tends to vanish from being significantly attractive (i.e., Fig. 9a) or repulsive (i.e., Fig. 9b) as the magnetite particles become farther apart. These two opposite trends due to the orientation of the field give rise to an interesting compromise as to how the separation between the magnetite particles enhances or weakens the attraction of the nanoparticle. For example, in the case where the field is oriented parallel to the y-axis (i.e., $\alpha = 0°$), the more separated the magnetite particles are, the more repulsive (or less attractive) the total force is on the nanoparticle anywhere in the defined x–y region. Note how in this case the interactions become more repulsive in the places where they are already repulsive (i.e., at the centers of the magnetite particles), and they become less attractive in the places where they are already attractive (i.e., at the middle regions between the magnetite particles). Exactly the opposite behavior results when the field is oriented parallel to the z-axis (i.e., $\alpha = 90°$). With larger distances between the magnetite particles, larger attractive interactions are observed in the zones where the forces are already attractive (i.e., at the centers) and less repulsive interactions are observed where the forces are already repulsive (i.e., at the middle regions). Of course, for all other orientations of the magnetic field, the observed behavior on the nanoparticle lies somewhere in between these two limits.

The consequence of these differing and opposing trends is that the distance between the magnetite particles does not provide a clear advantage in the design

Figure 9. z-Component of the total magnetic force on the paramagnetic nanoparticle that is exerted by the array of magnetite particles within the square defined in Fig. 1b for different distances between the magnetite particles (i.e., s), and for $h = 20$ nm and (a) $\alpha = 0°$ and (b) $\alpha = 90°$. All other parameters are fixed and given in Table 1.

of a magnetite-containing magnetic matrix for use in a packed HGMS column, because the angle α is distributed essentially randomly in such a situation. One thing that is clear, however, is the smoothing effect on the force over the nanoparticle that is caused by the close proximity of the magnetite particles. The force is decreased where single magnetite–nanoparticle interactions are expected to be strong, and increased where single magnetite–nanoparticle interactions are expected to be weak. Nevertheless, it is remarkable that despite this smoothing behavior, markedly strong magnetic forces still prevail, due to the presence of each single magnetite particle. The strongest interactions are realized at the (1,1), (1, − 1), (− 1,1), and (− 1, − 1) location, with somewhat weaker but still significant interactions realized at the (0,1), (0, − 1), (1,0), (− 1,0), and (0,0) location due to the multimagnetite synergism where single magnetite–nanoparticle interactions are expected to be weak. These results suggest, consequently, that a dense composite matrix containing magnetite particles as the magnetic media is entirely feasible, such as the 80 wt% magnetite–silica composite material developed recently by Ritter and coworkers.[9]

An important question that naturally arises from these results concerns the distance between the magnetite particles where the multi-particle effects of the matrix vanish. In other words, at what separation between the magnetite particles does the effect of the matrix diminish to the point where the interaction with the nanoparticle is essentially that corresponding to a single magnetite particle. Figures 10–12 answer this question by comparing each of the components of the total force on the nanoparticle (i.e., Figs. 10a, 11a, and 12a), with the z-component of the force resulting from a single magnetite particle (i.e., Figs. 10b, 11b, and 12b) at three different angles α (i.e., $\alpha = 0$, 45, and 90°), respectively. For the array, the z-component of the force is plotted within the square defined by the center of the magnetite particle at coordinate (− 1, − 1), the middle points between it and its neighboring magnetite particles (i.e., at (− 1,0) and (0, − 1)), and the coordinate (0,0) (see Fig. 1b). In Figs. 10b, 11b, and 12b, the single magnetite particle is assumed to be located at the same position of the magnetite particle in Figs. 10a, 11a, and 12a (i.e., at (− 1, − 1)). Notice how the surface-plots of the multi and single magnetite particles become nearly identical as s approaches 1.0 (i.e., as the magnetite to magnetite distance approaches two diameters). Hence, at distances larger than about two magnetite particle diameters, the nanoparticle effectively interacts only with one magnetite particle in the array, no matter what the orientation of the magnetic field be.

The importance of the surface-to-surface distance between the nanoparticle and the plane that is tangent to the surface of the magnetite particle array (i.e., h) on the force is disclosed in Fig. 13. Here, the variation of the z-component of the total force on the nanoparticle is plotted as a function of h for different values of s at four different values of α and at three different x–y coordinates (i.e., (0,0), (− 1,0), and (− 1, − 1). The graphs are characterized by the existence of strong

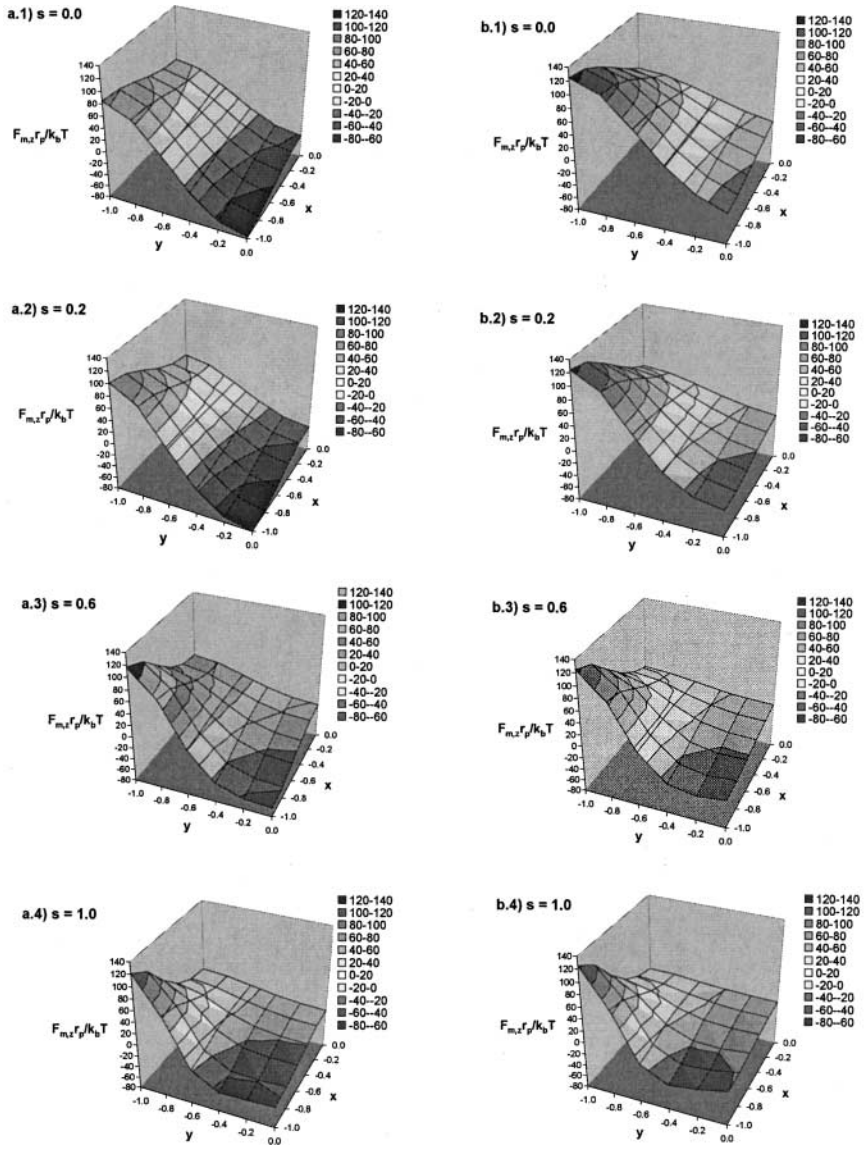

Figure 10. z-Component of the total magnetic force on the paramagnetic nanoparticle that is exerted by (a) the array of magnetite particles, and (b) a single magnetite particle at $(-1, -1)$ within the vicinity of the (x,y) coordinate $(-1, -1)$ for different separations of the magnetite particles (i.e., s) and for $h = 20\,\text{nm}$ and $\alpha = 0°$. All other parameters are fixed and given in Table 1.

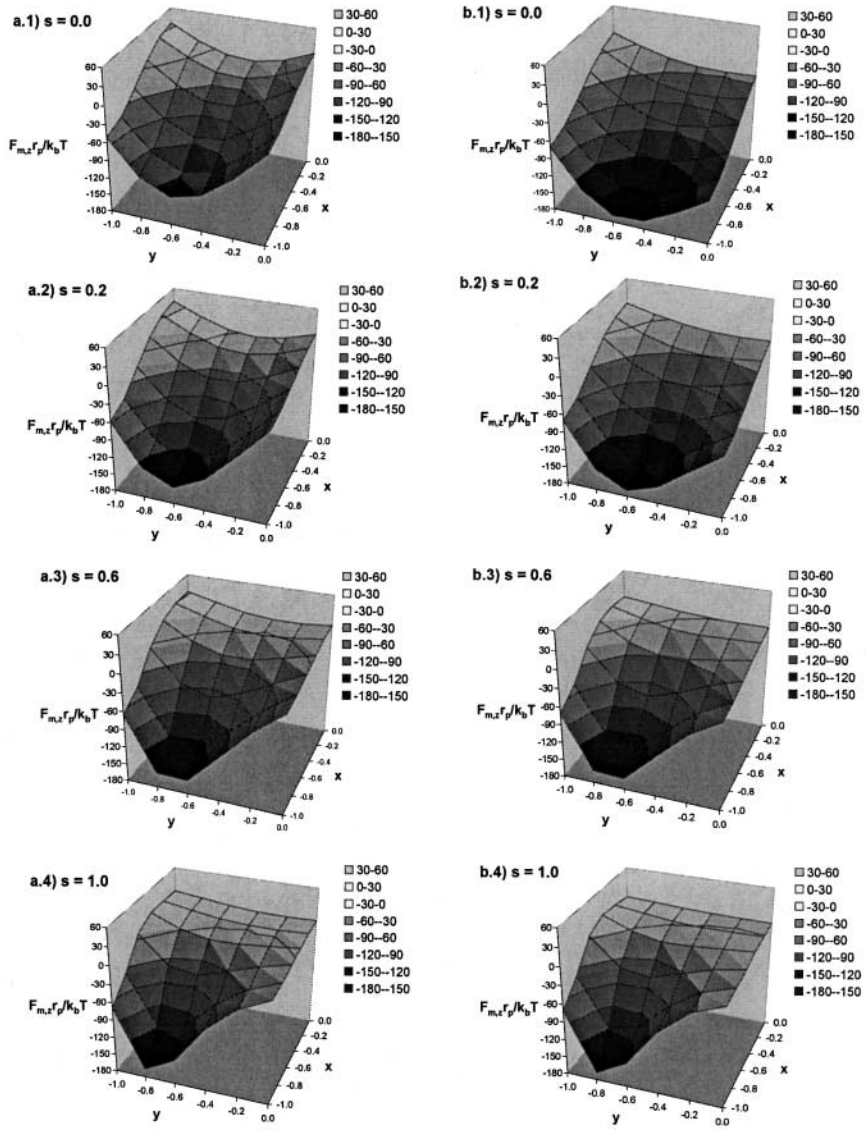

Figure 11. z-Component of the total magnetic force on the paramagnetic nanoparticle that is exerted by (a) the array of magnetite particles, and (b) a single magnetite particle at $(-1, -1)$ within the vicinity of the (x,y) coordinate $(-1, -1)$ for different separations of the magnetite particles (i.e., s) and for $h = 20\,\text{nm}$ and $\alpha = 45°$. All other parameters are fixed and given in Table 1.

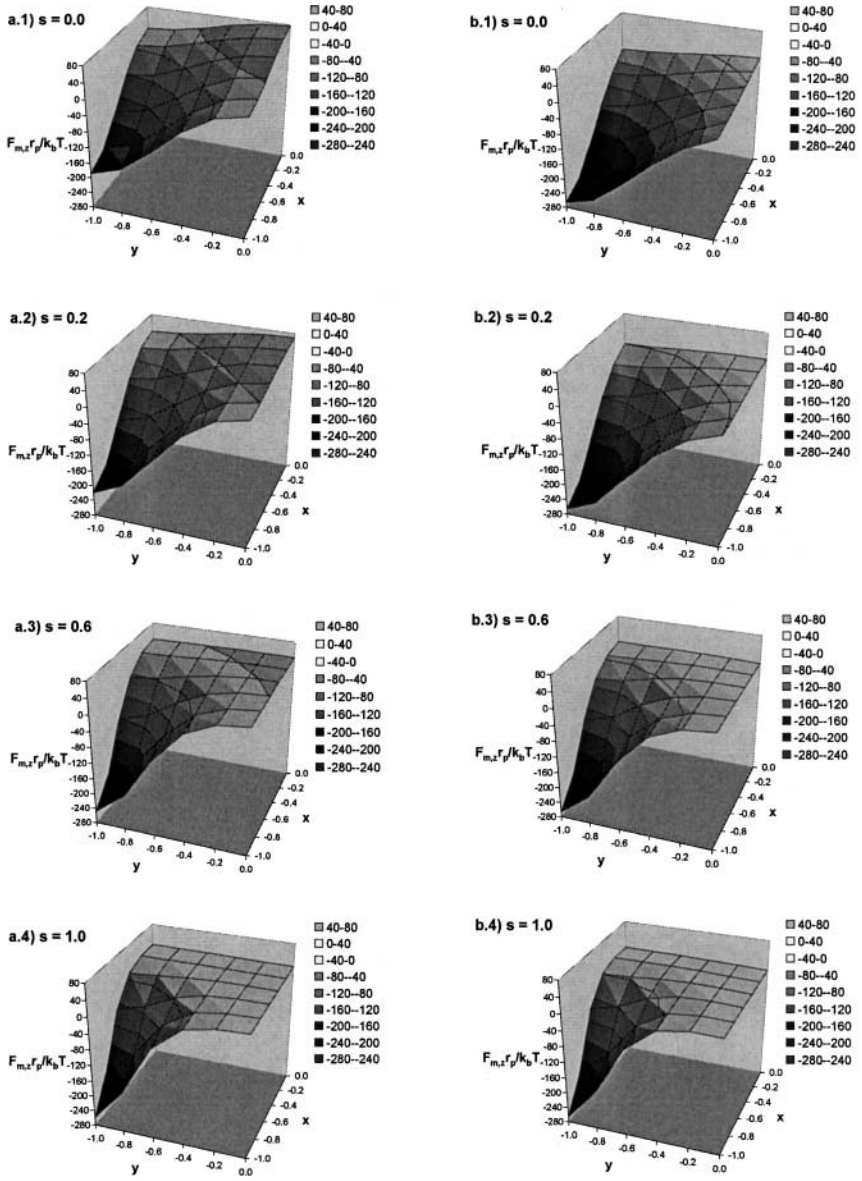

Figure 12. z-Component of the total magnetic force on the paramagnetic nanoparticle that is exerted by (a) the array of magnetite particles, and (b) a single magnetite particle at $(-1, -1)$ within the vicinity of the (x,y) coordinate $(-1, -1)$ for different separations of the magnetite particles (i.e., s) and for $h = 20$ nm and $\alpha = 90°$. All other parameters are fixed and given in Table 1.

forces in all of these conditions, but that decay rapidly within a surface-to-surface separation (i.e., h) of about 600 nm. It is particularly interesting, however, to observe that the same smoothing effects that caused the results discussed earlier are responsible for the leveling off of the forces at larger separations, which is especially evident when the magnetite particles are in contact. This minor variation with separation (i.e., flatness) and the fact that the forces are rather

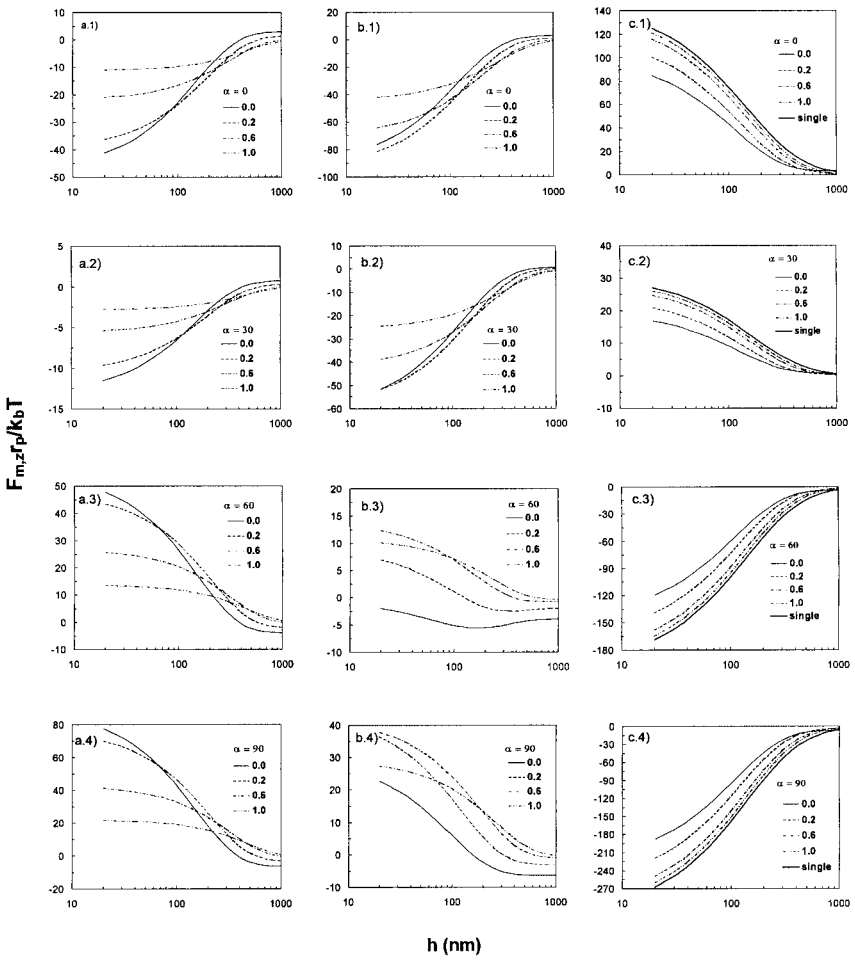

Figure 13. z-Component of the total magnetic force on the paramagnetic nanoparticle as a function of h for different distances between the magnetite particles (i.e., $s = 0.0$, 0.2, 0.6, and 1.0) and orientations of the magnetic field (i.e., α) at the (x,y) coordinate (a) (0,0), (b) $(-1,0)$, and (c) $(-1, -1)$. All other parameters are fixed and given in Table 1.

small (i.e., $F_{m,z}r_p/k_bT < 5$) is mainly a consequence of the smaller curvature associated with the entire array, which due to the close proximity among the magnetite particles, essentially behaves as a single large magnetite particle. Moreover, notice how this effect rapidly vanishes when the magnetite particles start to separate (i.e., at larger s values). For the nanoparticles studied here, and in general for any nanoparticle of a smaller size, these particular magnetic forces do not overcome the Brownian motion (due to the small values of $F_{m,z}r_p/k_bT$). Nevertheless, since the magnetic forces are strongly dependent on the size of the nanoparticle,[2–4] magnitudes of the forces in the second zone are expected to be strong enough to retain particles of a size comparable to that of the whole array. Consequently, the above results strongly suggest that a magnetite-containing magnetic matrix should not only be capable of attracting and retaining nanoparticles, but it should also be capable of removing larger particles with sizes in the order of a few microns. This is not necessarily the case for a single magnetite particle; hence, this result could not have been realized in the previous single magnetite particle studies.

As a concluding point, it is important to emphasize that, in general, both the magnetite and the nanoparticles contain acidic and basic groups that lead to the formation of charged surfaces when submerged in aqueous solutions. Consequently, the magnetic interactions discussed earlier are easily overcome by electrostatic interactions between these two species, if special precautions are not taken.[2,4] Fortunately, the range over which the electrostatic forces operate is strongly dependent on the concentration of the background electrolyte in solution; therefore, they are easily controlled. For example, at concentrations higher than 0.01 M of a symmetric 1:1 background electrolyte, the electrostatic interactions are suppressed and ineffective at values of h greater than 30 nm. This permits the magnetic forces, with magnitudes typical of that observed in this work, to operate over a range of h where the nanoparticles are effectively attracted to and retained by the magnetite array.[4]

CONCLUSIONS

The magnetic force between a paramagnetic nanoparticle and a 3-D array of magnetite particles was investigated. Three important parameters were studied: the separation between the magnetite particles in the array, the orientation of the magnetic field, and the distance between the nanoparticle and the surface of the magnetite array. Independent of the orientation of the magnetic field, zones of attractive interactions between the array and the nanoparticle were always present, and they moved along the lines of centers between the magnetite particles that were parallel to the plane of the field. This was not the case in the single magnetite particle studies, where repulsive zones also existed for certain

orientations of the magnetic field. However, compromising effects were observed as a consequence of the effect of the array. For example, when the magnetic field was parallel to the face of the array (i.e., $\alpha = 0°$), the attractive zones were located in the middle points of the line of centers, and the force on the nanoparticle was enhanced as the magnetite particles became closer to each. This indicated that the neighboring magnetite particles played a positive role in increasing the attractive force on the nanoparticle. In contrast, when the magnetic field was perpendicular to the face of the array (i.e., $\alpha = 90°$) the attractive zones were located just in front of each magnetite particle and in this case the force became stronger with larger, as opposed to smaller, separations between the magnetite particles. This indicated that the neighboring magnetite particles played a negative role in decreasing the attractive force on the nanoparticle. Both situations were consequence of the so-called smoothing effect associated with the array. For any other angle of the magnetic field, compromising trends in between these two extremes were observed. Nevertheless, at separations larger than two magnetite diameters between the magnetite particles, the force on the nanoparticle was essentially that due to just one of the magnetite particles in the array; therefore, the smoothing effect of the array was lost. In general, as long as the magnetite particles are less than two diameters apart, when the distance between the nanoparticle and the array increases from zero to great distances (i.e., $h > 600\,\text{nm}$), the magnetic force changes from being strong, which results from the curvature of a single magnetite particle, to being weak and particularly flat when magnetite particles are in contact with each other. This latter situation is when the magnetite particle behaves as one much larger particle (i.e., small curvature). Although for the nanoparticle studied here, these forces at large separations were insufficient to secure retention, they are expected to be sufficiently strong for retention of particles that are of sizes comparative to the size of the array. Overall, these results suggested that a magnetic matrix, comprising clumps of magnetite particles, should be effective at attracting and retaining not only nanoparticles down to 40 nm in radius due to individual magnetite-particle effects, but also nanoparticles with radii in the order of a few microns due to multi-magnetite particle effects. In contrast, a typical stainless steel wire matrix would have difficulty attracting and retaining such small, weakly paramagnetic nanoparticles in an HGMS process.

NOMENCLATURE

$F^*_{\text{m},i}$	j-coordinate of the dimensionless magnetic force between the paramagnetic nanoparticle and the array of magnetite particles applied to the system of coordinates x, y, and z (N)

$F_{m,i}$	j-coordinate of the magnetic force between the paramagnetic nanoparticle and the array of magnetite particles applied to the system of coordinates x, y, and z (N)
$F_{m,i,j}$	j-coordinate of the magnetic force between the paramagnetic nanoparticle and magnetite particle i applied to any system of coordinates (N)
$F_{m,r}$	radial component of the magnetic force between a magnetite particle and a paramagnetic nanoparticle with the origin at the center of the magnetite particle (N)
$F_{m,\theta}$	angular component of the magnetic force between a magnetite particle and a paramagnetic nanoparticle with the origin at the center of the magnetite particle (N)
h	surface-to-surface distance between the paramagnetic nanoparticle and the plane that is tangent to the top layer of the magnetite particles in the array and parallel to the $x-y$ plane (m)
$\mathbf{H}_a$	vector form of the externally applied magnetic field ($A\,m^{-1}$)
H_a	scalar form of the externally applied magnetic field ($A\,m^{-1}$)
k_b	Boltzmann constant, 1.3807×10^{-23} ($J\,K^{-1}$)
k_i	index corresponding to magnetite particle i in the x-direction
l_i	index corresponding to magnetite particle i in the y-direction
m_i	index corresponding to magnetite particle i in the z-direction
M_s	saturation magnetization of magnetite ($A\,m^{-1}$)
N	number of magnetite particles in the array
r	center-to-center distance between the paramagnetic nanoparticles and a magnetite particle; radial coordinate in the spherical coordinate system (m)
r_m	radius of a magnetite particle (m)
r_p	radius of a paramagnetic nanoparticle (m)
s	ratio between the surface-to-surface distance between the magnetite particles and their diameter
T	temperature (K)
V_p	volume of the paramagnetic nanoparticle (m^3)
x	dimensionless form of X_p^* according to Eq. (14a)
X_i^*	x-coordinate of the paramagnetic nanoparticle relative to the center of magnetite particle i (m)
$X_{m,i}^*$	x-coordinate of magnetite particle i with respect to the origin defined in Fig. 2b (m)
X_p^*	x-coordinate of the paramagnetic nanoparticle with respect to the origin defined in Fig. 2b (m)
$X_i'^*$	x-coordinate of the paramagnetic nanoparticle relative to the center of magnetite particle i, in the auxiliary Cartesian coordinate system depicted in Fig. 3 (m)

y	dimensionless form of Y_p^* according to Eq. (14b)
Y_i^*	y-coordinate of the paramagnetic nanoparticle relative to the center of magnetite particle i (m)
$Y_{m,i}^*$	y-coordinate of the magnetite particle i with respect to the origin defined in Fig. 2b (m)
Y_p^*	y-coordinate of the paramagnetic nanoparticle with respect to the origin defined in Fig. 2b (m)
$Y_i'^*$	y-coordinate of the paramagnetic nanoparticle relative to the center of magnetite particle i, in the auxiliary Cartesian coordinate system depicted in Fig. 3 (m)
Z_i^*	z-coordinate of the paramagnetic nanoparticle relative to the center of magnetite particle i (m)
$Z_{m,i}^*$	z-coordinate of the magnetite particle i with respect to the origin defined in Fig. 2b (m)
Z_p^*	z-coordinate of the paramagnetic nanoparticle with respect to the origin defined in Fig. 2b (m)
$Z_i'^*$	z-coordinate of the paramagnetic nanoparticle relative to the center of magnetite particle i, in the auxiliary Cartesian coordinate system depicted in Fig. 3 (m)
α	angle between the y-axis and the applied magnetic field H_a, in the plane parallel to the $z-y$ plane as depicted in Fig. 1
χ_m	volumetric magnetic susceptibility of the medium
χ_p	volumetric magnetic susceptibility of the paramagnetic nanoparticle
ϕ_i	azimuthal angular coordinate in the spherical coordinate system defined in Fig. 4, with the origin at the center of magnetite particle i
μ_0	magnetic permeability of free space, $4\pi \times 10^{-7}$ (T m A^{-1})
θ	angular coordinate in the spherical coordinate system
θ_i	polar angular coordinate in the spherical coordinate system defined in Fig. 4, with the origin at the center of magnetite particle i

ACKNOWLEDGMENT

The authors gratefully acknowledge the financial support from the National Science Foundation under Grant No. CTS-9985489.

REFERENCES

1. Kochen, R.L.; Navratil, J.D. Removal of Radioactive Materials and Heavy Metals from Water Using Magnetic Resin. US Patent 5,595,666, 1997.
2. Ebner, A.D.; Ritter, J.A.; Ploehn, H.J. Feasibility and Limitations of Nanolevel High Gradient Magnetic Separation. Sep. Purif. Technol. **1997**, *11*, 199.
3. Ebner, A.D.; Ritter, J.A.; Ploehn, H.J.; Kochen, R.L.; Navratil, J.D. New Magnetic Field-Enhanced Process for the Treatment of Aqueous Wastes. Sep. Sci. Technol. **1999**, *34*, 1277.
4. Ebner, A.D.; Ritter, J.A.; Ploehn, H.J. Magnetic Hetero-flocculation of Paramagnetic Colloidal Particles. J. Colloid Interface Sci. **2000**, *225*, 39.
5. Badescu, V.; Rotariu, O.; Murariu, V.; Rezlescu, N. Transverse High Gradient Magnetic Filter with Bounded Flow Field. IEEE Trans. Magn. **1997**, *33*, 4439.
6. Hayashi, E.; Uchiyama, S. On the Trajectory and Capture Efficiency Around Many Wires. IEEE Trans. Magn. **1980**, *16*, 827.
7. Eisenstein, I. Magnetic Traction Force in an HGMS with an Ordered Array of Wires: II. IEEE Trans. Magn. **1978**, *14*, 1155.
8. Eisenstein, I. Magnetic Traction Force in an HGMS with an Ordered Array of Wires: I. IEEE Trans. Magn. **1978**, *14*, 1148.
9. Shen, J.C.; Ebner, A.D.; Ritter, J.A. Points of Zero Charge and Intrinsic Equilibrium Constants of Silica–Magnetite Composite Oxides. J. Colloid Interface Sci. **1999**, *214*, 333.

Received September 2001
Revised January 2002